

Adiabatic passage in photon-echo quantum memories

Gabor Demeter*

Wigner Research Center for Physics, Hungarian Academy of Sciences, Konkoly-Thege Miklós út 29-33, H-1121 Budapest, Hungary

(Received 2 September 2013; revised manuscript received 24 October 2013; published 15 November 2013)

Photon-echo-based quantum memories use inhomogeneously broadened, optically thick ensembles of absorbers to store a weak optical signal and employ various protocols to rephase the atomic coherences for information retrieval. We study the application of two consecutive, frequency-chirped control pulses for coherence rephasing in an ensemble with a “natural” inhomogeneous broadening. Although propagation effects distort the two control pulses differently, chirped pulses that drive adiabatic passage can rephase atomic coherences in an optically thick storage medium. Combined with spatial phase-mismatching techniques to prevent primary echo emission, coherences can be rephased around the ground state to achieve secondary echo emission with close to unit efficiency. Potential advantages over similar schemes working with π pulses include greater potential signal fidelity, reduced noise due to spontaneous emission, and better capability for the storage of multiple memory channels.

DOI: [10.1103/PhysRevA.88.052316](https://doi.org/10.1103/PhysRevA.88.052316)

PACS number(s): 03.67.Hk, 42.50.Gy, 42.50.Md, 42.50.Ex

I. INTRODUCTION

Building a quantum memory for light is vital for creating future large-scale quantum-communication networks and essential for several devices in quantum-information processing. We must store the quantum state of light in some material device and be able to retrieve it efficiently and faithfully. Thus intense research is going on to create an optical memory that could work right down to the single-photon level, using several different approaches [1,2]. In particular, photon-echo-based techniques have been investigated extensively [3].

The first essential ingredient for any optical memory based on the photon-echo principle is an inhomogeneously broadened ensemble of “atoms” that absorb the signal and dephase for storage. Rare-earth-ion dopants embedded in solid-state lattices are a popular choice because they have very long coherence times at low temperatures, the density of absorbers can be very large, and decoherence due to atomic motion is absent. The second essential ingredient is a protocol to collectively rephase the atomic coherences of the ensemble for the retrieval of the signal echo. The numerous techniques can be categorized in two wide groups. The first one uses an atomic ensemble with a “natural” inhomogeneous broadening and one or more strong control pulses to rephase the coherences in the spirit of the classical photon-echo phenomenon [4]. The second group uses specially prepared atomic ensembles, whose absorption line shapes are crafted prior to signal absorption.

The simplest technique of the first category is the classical two-pulse photon echo. It uses a single short π pulse to rephase the coherences and does not require any initial state preparation of the ensemble. However, Ruggiero and co-workers showed [5] that it is unsuitable for a quantum-memory protocol for several reasons. First, rephasing occurs when the ensemble is inverted, severely limiting the signal-to-noise ratio during quantum-state retrieval. Second, the control pulse is distorted during propagation, its bandwidth decreases gradually, and it

develops a long tail that may interfere with the detection of the echo [6]. Furthermore, the protocol is extremely sensitive to the precise preparation of the control pulse, as the pulse area of π is in fact an unstable solution of the famed area equation. Third, a control pulse whose bandwidth is wide enough to rephase the coherences of the ensemble must be very short, with a high peak intensity, which may well exceed the damage threshold in a crystal.

Noise from an inverted storage medium prevents quantum-information storage in other cases as well [7], so techniques were proposed to prevent the emission of the first echo and use a second control pulse to rephase the coherences again. This secondary echo (in fact an echo of the primary echo) is emitted when the atomic dipoles rephase around the ground state. Damon and co-workers [8] used the fact that if signal and control pulses propagate in different directions, the primary echo fails the phase-matching condition, so it is silenced—a technique also employed in [9]. Another protocol [10] uses a third atomic level and strong Raman-type interaction to store the signal in the coherences between the two stable states. It employs special writing, rephasing, and reading pulses to achieve rephasing around the ground state. An auxiliary electrical field gradient that broadens the absorption line during the first rephasing can also be used to silence the primary echo [11].

Techniques belonging to the second group achieve coherence rephasing around the ground state by preparing a special absorption feature in the storage medium. Controlled reversible inhomogeneous broadening (CRIB) [3,12–14] and gradient echo memory [15,16] techniques use a narrow absorption line broadened by an externally applied inhomogeneous field. Reversing the field gradient rephases the atoms, so inverting them is not necessary. These techniques have been demonstrated to work in solid-state media [17–19] and used in more elaborate configurations such as information storage in Raman coherences [20,21] or polarization-state qubit storage in three-level systems [22,23]. Another technique is to craft an absorption feature composed of narrow, equidistant peaks termed atomic frequency combs (AFCs) [24–26]. Atomic coherences then spontaneously rephase periodically, with a

*demeter.gabor@wigner.mta.hu

period given by the frequency spacing of the peaks. The greatest difficulty with these techniques is the preparation of the required absorption feature with sufficient optical depth.

As for techniques of the first category that use an unmanipulated absorption line, silencing the primary echo still does not solve problems associated with control-pulse propagation in an optically dense medium, such as pulse distortion, high peak intensity, and sensitivity to the precise pulse area. Recently, frequency-chirped control pulses that drive adiabatic passage (AP) between the atomic states were proposed for use in photon-echo quantum memories [8,26,27]. It has been shown that while AP with a single chirped pulse cannot, in general, rephase the coherences collectively, a pair of consecutive APs can under certain conditions, most notably when the control pulses are identical. With chirped control pulses, the precise pulse area is not important and they can invert the same frequency range of the atomic ensemble using much smaller peak intensities than π pulses. For this reason, AP demonstrates superior performance compared to π pulses also in rephasing coherences in quantum memory experiments based on electromagnetically induced transparency [28]. However, the question of pulse propagation effects remains. Even if the control pulses are identical at the entry of the medium, they will surely be different at finite optical depths, because the second one propagates in a gain medium inverted by the first one. For a collective rephasing of the coherences, it is not only population transfer that counts, but also the time integral of the adiabatic eigenvalues [26,27]. So how do pulse propagation effects modify the ability of a pair of chirped control pulses to rephase atomic coherences?

In this paper we investigate the propagation properties of two consecutive, frequency-chirped control pulses in an optically thick, inhomogeneously broadened atomic ensemble. Calculating the distortion that the control pulses undergo, we investigate their ability to collectively rephase the coherences of the ensemble. We also compare their performance to that of a pair of π control pulses. We show that chirped control pulses are much more suitable for rephasing an optically thick storage medium for multiple reasons. Finally, we calculate the echo of a series of weak signal pulses and characterize the efficiency and fidelity of an optical memory with chirped control pulses. We prove that together with phase mismatching to extinguish the primary echo, frequency-chirped control pulses can be used effectively in optical quantum memories.

II. BASIC PRINCIPLES

We consider two variants of a photon-echo memory protocol in which an unmanipulated, natural inhomogeneously broadened absorption line is used for storage, and two consecutive control pulses drive AP in the ensemble twice to rephase the coherences around the ground state. The general timelines of the variants are depicted in Fig. 1. In the first one, we simply use an ensemble of two-level atoms and two control pulses. In the second variant, we assume that an additional pair of counterpropagating pulses transfer the excited-state population to a third, long-lived state $|s\rangle$ just after signal absorption as in several other protocols (e.g., [26]). This step can extend storage time and perform phase matching to enable backward echo emission. We envision a solid-state medium

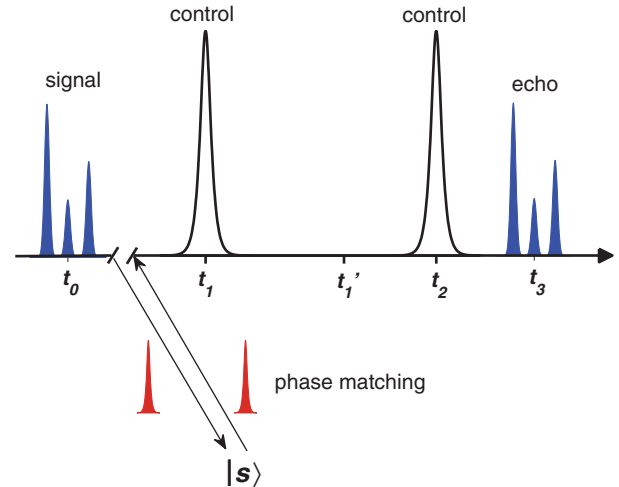


FIG. 1. (Color online) Interaction timeline. A signal field at t_0 is followed by two consecutive control pulses at t_1 and t_2 , with the echo emission occurring at t_3 . The primary echo at t'_1 is silenced by spatial phase mismatching. In a variant of the protocol, a pair of counterpropagating pulses can be used to transfer atomic populations between the excited state and a third, stable state to achieve longer storage times and obtain phase matching for backward echo emission.

where inhomogeneous broadening is independent of the pulse propagation direction, and assume that $L \gg \lambda$ is fulfilled for the length L of the storage medium, so the primary echo can be silenced using spatial phase mismatching [8]. We restrict our consideration to signal- and control-pulse propagation along a single dimension. The reason is that the interaction region where the signal is absorbed in photon-echo memory experiments is usually highly elongated, so achieving AP with control pulses at an angle would probably require pulses with prohibitively large intensities and/or very oblique beam shapes. Finally, we assume that the signal field is so weak (a few-photon pulse) that it does not, in any way, interfere with control pulse propagation, i.e., this can be computed in the “empty” medium and the results then used to calculate the triggering of echoes.

A. Basic equations

We consider propagation along a single direction and write the electric field as a sum of forward- and backward-propagating modes, so the (classical) electric field is

$$E(z,t) = \frac{1}{2}[E_f(z,t)e^{ikz-\omega_0t} + E_b(z,t)e^{-ikz-\omega_0t} + \text{c.c.}]$$

with the slowly varying envelope functions $E_f(z,t)$ and $E_b(z,t)$. Here ω_0 is the central frequency of the inhomogeneously broadened absorption line and we use the time-dependent complex phase of the envelope functions to include detunings and frequency modulations in our description.

We use the rotating-frame Hamiltonian $\hat{H}_a = \hbar\Delta|e\rangle\langle e|$ to describe a two-level system with transition frequency $\omega_{eg} = \omega_0 + \Delta$, offset by Δ from the inhomogeneously broadened line center. In addition, we use the standard dipole interaction Hamiltonian and the rotating-wave approximation. Thus we obtain the following equations for the probability amplitudes $\alpha(t; z, \Delta)$, $\beta(t; z, \Delta)$ that describe the state of an atom at point

z as $|\psi\rangle = \alpha(t; z, \Delta)|g\rangle + \beta(t; z, \Delta)|e\rangle$:

$$\begin{aligned}\partial_t \alpha(t; z, \Delta) &= \frac{i}{2} [\Omega_f^*(t, z) e^{-ikz} + \Omega_b^*(t, z) e^{ikz}] \beta(t; z, \Delta), \\ \partial_t \beta(t; z, \Delta) &= \frac{i}{2} [\Omega_f(t, z) e^{ikz} + \Omega_b(t, z) e^{-ikz}] \alpha(t; z, \Delta) \\ &\quad - i \Delta \beta(t; z, \Delta).\end{aligned}$$

Here $\Omega_{f,b} = dE_{f,b}/\hbar$ are the Rabi frequencies of the forward- and backward-propagating fields with $d = \langle e|\hat{d}|g\rangle$ the dipole matrix element. We have neglected all decay processes in this description, so the overall interaction time must be much shorter than any atomic population or coherence decay times. It is convenient to decompose the probability amplitudes as a series of spatial Fourier modes:

$$\begin{aligned}\alpha(t; z, \Delta) &= \sum_n \alpha_n(t; z, \Delta) e^{inkz}, \\ \beta(t; z, \Delta) &= \sum_n \beta_n(t; z, \Delta) e^{inkz}.\end{aligned}$$

$\alpha_n(t; z, \Delta)$ and $\beta_n(t; z, \Delta)$ still depend on z , but now vary only slowly on the scale of the light wavelength, similarly to $\Omega_{f,b}$. Using $kL \gg 1$, we can separate the evolution equation for the slowly varying probability amplitudes:

$$\begin{aligned}\partial_t \alpha_n &= \frac{i}{2} (\Omega_f^* \beta_{n+1} + \Omega_b^* \beta_{n-1}), \\ \partial_t \beta_n &= \frac{i}{2} (\Omega_f \alpha_{n-1} + \Omega_b \alpha_{n+1}) - i \Delta \beta_n.\end{aligned}\quad (1)$$

(The explicit dependence on t , z , and Δ has been suppressed for brevity.)

To obtain the spatiotemporal evolution of the fields from the wave equation, we employ the slowly varying envelope approximation. Using $kL \gg 1$, the equations for $\Omega_f(z, t)$ and $\Omega_b(z, t)$ can be separated:

$$\begin{aligned}\left(\frac{1}{c} \partial_t + \partial_z\right) \Omega_f(t, z) &= i \frac{\alpha_d}{\pi g(0)} \mathcal{P}_1(z, t), \\ \left(\frac{1}{c} \partial_t - \partial_z\right) \Omega_b(t, z) &= i \frac{\alpha_d}{\pi g(0)} \mathcal{P}_{-1}(z, t).\end{aligned}\quad (2)$$

Here $g(\Delta)$ is the inhomogeneous line shape function, $\alpha_d = \pi g(0) k \mathcal{N} d^2 / \varepsilon_0 \hbar$ is the absorption constant, and we have introduced the notation

$$\mathcal{P}_{\pm 1}(z, t) = \int \sum_n \alpha_n^* \beta_{n\pm 1} g(\Delta) d\Delta \quad (3)$$

for the forward and backward parts of the polarization. The fact that each field interacts only with the corresponding part of the polarization is an expression of the spatial phase-matching condition. Equations (1) and (2) together with (3) constitute the set of Maxwell-Bloch equations for our case. They can be solved analytically for the signal field in the weak-excitation limit [5], but can only be solved numerically for the control pulses and for the echo. However, we assume that the pulses propagate in complete time separation, so the solution is somewhat simplified—during the time interval $[t_i - T, t_i + T]$ where the i th pulse has a finite amplitude, it is enough to solve Eqs. (1) for one or two pairs of amplitudes $\{\alpha_n, \beta_{n\pm 1}\}$ that Ω_i couples, those that may be nonzero at the time of the i th

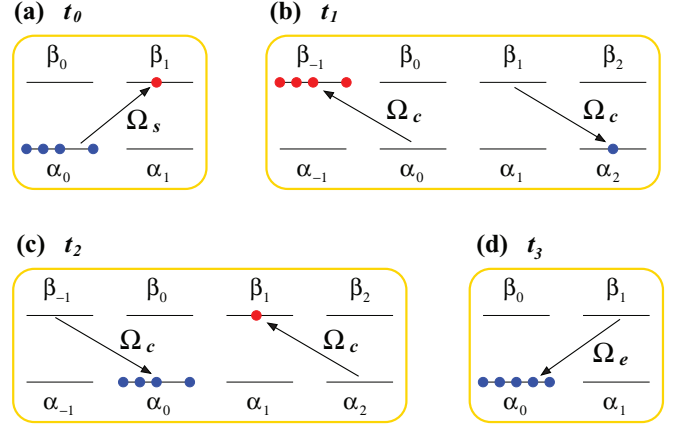


FIG. 2. (Color online) Steps of the first memory variant showing the populated probability amplitudes and the transfers driven by the various fields. Two backward-propagating control pulses rephase the coherences around the ground state and a forward echo is emitted.

pulse and may contribute to $\mathcal{P}_{\pm 1}$. In the second variant of the protocol where two additional pulses transfer the atomic excitation between $|e\rangle$ and a third state $|s\rangle$, we simply assume that they are perfect π pulses or a pair of identical chirped pulses. Because the $|e\rangle \leftrightarrow |s\rangle$ transition is virtually empty in the case of weak signal fields, the medium is perfectly transparent for these pulses, and propagation effects need not be taken into account for them.

B. Primary echo suppression via spatial phase mismatching

The main steps of the two variants are sketched in Figs. 2 and 3, which depict the various probability amplitudes that differ from zero at certain times. Assuming that we start with a spatially homogeneous medium, initially only α_0 is nonzero. In the first case, the absorption of the forward-propagating signal pulse at t_0 creates coherences in the $\{\alpha_0, \beta_1\}$ amplitude pair [Fig. 2(a)]. The first control pulse at t_1 , which propagates in the backward direction, inverts the atoms, transferring the populations to β_{-1} and α_2 [Fig. 2(b)]. When coherences rephase around the excited state at t_1' the polarizations \mathcal{P}_1 and \mathcal{P}_{-1} are both zero—indeed only \mathcal{P}_{-3} is nonzero—so the primary echo is silenced. At t_2 the second control pulse (backward propagating) returns the populations to $\{\alpha_0, \beta_1\}$ [Fig. 2(c)], so the rephasing at t_3 occurs around the ground state, giving rise to \mathcal{P}_1 , i.e., forward echo emission [Fig. 2(d)].

The first step of the second variant is identical to the first one [Fig. 3(a)], but now it is followed by a transfer of the excited-state population to the shelving state $|s\rangle$ by a forward-propagating pulse [Fig. 3(b)]. The dephasing is halted and the signal stored in the coherence between $\{\alpha_0, \gamma_0\}$ as in other protocols [10,26]. Upon demand a second pulse, this time backward propagating, transfers the population from γ_0 to β_{-1} , and rephasing can proceed. We assume that the difference between the wavelengths of the control-pulse pair driving the shelving transition $|e\rangle \leftrightarrow |s\rangle$ and the signal field is small ($|k_c - k_s|L \ll 1$), so this pulse pair also performs the necessary phase matching required for backward echo emission. Because this transition is virtually empty, we simply assume them to be a pair of identical chirped pulses and

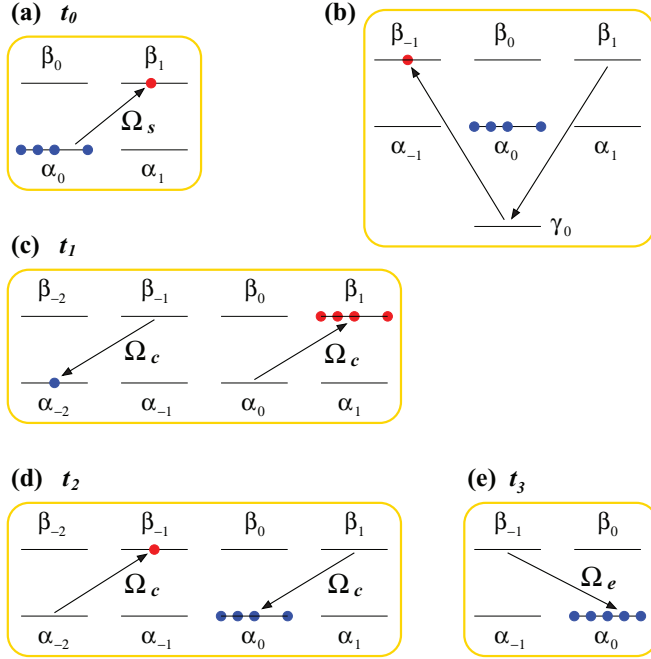


FIG. 3. (Color online) Steps of the second memory variant showing the populated probability amplitudes and the transfers driven by the various fields. A pair of counterpropagating pulses on the $|e\rangle \leftrightarrow |s\rangle$ transition and two forward-propagating control pulses rephase the coherences around the ground state and a backward echo is emitted.

need not consider their propagation. Next, the first control pulse at t_1 , this time forward propagating, inverts the atoms, transferring the populations to β_1 and α_{-2} [Fig. 3(c)]. When the coherences rephase around the excited state at t'_1 , only \mathcal{P}_3 is nonzero. Rephasing occurs at t_3 , after the second control pulse [Fig. 3(d)] giving rise to \mathcal{P}_{-1} , i.e., a backward echo is generated [Fig. 3(e)]. Note, however, that because of possible imperfections in the population transfer process, we must in fact use more amplitude pairs than depicted in Figs. 2 and 3 when computing echo emission numerically.

III. COHERENCE REPHASING WITH ADIABATIC PASSAGE

A. Properties of the time-evolution operator

The control pulses at t_1 and t_2 must be able to rephase a sufficiently large region of the atomic ensemble in terms of optical depth and frequency range in order to trigger echo emission with high efficiency and good fidelity. To investigate whether the coherences imprinted by the signal can be rephased by the pulses, we construct the time-evolution operator $\hat{U}(\Delta, z)$ that connects the values of a pair of probability amplitudes at $t = t_3 - T$ just before echo emission with their values at $t = t_0 + T$ just after the signal pulse has been absorbed:

$$\begin{pmatrix} \alpha'_n \\ \beta'_{n\pm 1} \end{pmatrix} = \hat{U}(\Delta, z) \begin{pmatrix} \alpha_n \\ \beta_{n\pm 1} \end{pmatrix}.$$

(The upper sign in $\beta_{n\pm 1}$ is valid for forward-propagating control pulses, and the lower sign for backward ones.) $\hat{U}(\Delta, z)$ can be constructed from the time-evolution matrices $\hat{U}^{C1}(\Delta, z)$

and $\hat{U}^{C2}(\Delta, z)$ of the two control pulses that propagate the amplitudes during the time intervals $[t_{1,2} - T', t_{1,2} + T']$ and the free-evolution matrices between the various pulses. (See the Appendix for a short derivation, or [27] for a detailed treatment.)

Let us now define the quantities \mathcal{R}^{C1} and \mathcal{R}^{C2} using the off-diagonal matrix elements of $\hat{U}^{Cj}(\Delta, z)$, $j \in \{1, 2\}$:

$$\mathcal{R}^{Cj}(\Delta, z) = [\hat{U}^{Cj}(\Delta, z)]_{12} [\hat{U}^{Cj}(\Delta, z)]_{21}^*.$$

Clearly, $\mathcal{R}^{Cj}(\Delta, z)$ is the quantity that is relevant for the collective rephasing of coherences by the j th control pulse. First, its magnitude gives the probability that the control pulse inverts the atomic states. Second, $|\mathcal{R}^{Cj}(\Delta, z)| = 1$ implies $[\hat{U}^{Cj}(\Delta, z)]_{11} = [\hat{U}^{Cj}(\Delta, z)]_{22} = 0$, so in this case the atomic coherences are transformed by the pulse during the time interval $[t_j - T', t_j + T']$ as

$$(\alpha_n^* \beta_{n\pm 1})' = (\mathcal{R}^{Cj}(\Delta, z) \alpha_n^* \beta_{n\pm 1})^*.$$

For a perfect π pulse, $\mathcal{R}^{Cj} = 1$, while for a control pulse that creates AP between the two atomic states

$$\mathcal{R}^{Cj}(\Delta, z) = -e^{i[\Lambda_j^- + \Phi_j(t_j - T')]} e^{i[-\Lambda_j^+ + \Phi_j(t_j + T')]} \quad (4)$$

[see Eq. (A6)]. Here Λ_j^\pm are the time integrals of the adiabatic eigenvalues for the duration of the control pulse which depend explicitly on Δ and, through the complex pulse amplitude $\Omega_j(z, t)$ which changes as the control pulse propagates, also on z . $\Phi_j(t)$ is the complex phase of $\Omega_j(z, t)$. In general, a single control pulse is able to collectively rephase the coherences in some region of the ensemble if, in this domain of Δ and z , both $|\mathcal{R}^{Cj}(\Delta, z)| = 1$ and $\arg[\mathcal{R}^{Cj}(\Delta, z)] = \text{const}$ are satisfied simultaneously. This is usually not the case. (Rephasing is possible when the control-pulse amplitude is so large that the dependence of Λ_j^\pm on Δ is negligible, but this presents the same problems with peak intensity as a short π pulse.)

When two chirped control pulses are used in succession for rephasing, both of which create AP, the overall transformation of the atomic coherences becomes

$$\begin{aligned} (\alpha_n^* \beta_{n\pm 1})' &= (\alpha_n^* \beta_{n\pm 1}) [\hat{U}(\Delta, z)]_{11}^* [\hat{U}(\Delta, z)]_{22} \\ &= (\alpha_n^* \beta_{n\pm 1}) \mathcal{R}^{C1}(\Delta, z) [\mathcal{R}^{C2}(\Delta, z)]^* \\ &\quad \times e^{i\Delta(2t_2 - 2t_1 + t_0 - t_3 + 2T)} \end{aligned} \quad (5)$$

[see Eqs. (A7)—we stress again that this formula is valid only when both pulses create AP]. From Eq. (5) it is clear that a pair of chirped control pulses can rephase atomic coherences collectively even if a single one cannot [26,27]. If $|\mathcal{R}^{C1}| = |\mathcal{R}^{C2}| = 1$ and $\arg(\mathcal{R}^{C1}) = \arg(\mathcal{R}^{C2}) + 2m\pi$ are both satisfied simultaneously, coherences will be just prepared for rephasing at t_3 by the control pulses provided that $2t_2 - 2t_1 + t_0 - t_3 = 0$. At the entry of the storage medium, this can easily be achieved by the use of two identical control pulses. But the two control pulses will be deformed during propagation in a different way, because they experience different initial conditions. The first pulse is absorbed, while the second one propagates through an inverted medium and is thus amplified. Thus we must also investigate just how fast propagation effects destroy the capability of the control-pulse pair to rephase.

B. Simulation results

To investigate whether a pair of control pulses would be able to rephase an optically thick ensemble of two-level atoms, we solved Eqs. (1)–(3) for a pair of propagating chirped control pulses using a computer. We used control pulses of the form

$$\Omega(0, t) = \Omega_0 [\text{sech}(t/\tau)]^{1+i\mu}, \quad (6)$$

which yield a time-dependent detuning from the atomic line center as

$$\partial_t \Phi(0, t) = -\frac{\mu}{\tau} \tanh\left(\frac{t}{\tau}\right). \quad (7)$$

For $\mu = 0$, there is no chirp and the pulse area is $\mathcal{A} = \pi\Omega_0/\tau$, while for $\mu \neq 0$ the chirp ranges from μ/τ to $-\mu/\tau$. Before the first control pulse, all atoms are in the ground state, while the second one propagates through the medium prepared by the first one—atomic excitations remain, but the coherences have had time to dephase. Having obtained $\Omega_j(z, t)$ we constructed the operators $\hat{U}^{Cj}(z, t)$ to investigate its matrix elements as a function of Δ and z . We considered two different cases. In one, the inhomogeneous broadening of the atomic line is much larger than the pulse bandwidth, so $g(\Delta) = g_0$ is taken to be constant. In this case the pulses are able to invert only a part of the ensemble, leaving atoms with a large Δ untouched. Clearly, there is then a transition region where the control pulses interact with the atoms but AP is not perfect. In the other case, we have a Gaussian line shape function $g(\Delta) = \exp(-\Delta^2/2\sigma_\Delta^2)/\sigma_\Delta\sqrt{2\pi}$ and the control-pulse bandwidth is great enough to encompass the whole absorption line. The first of these two cases is especially interesting, as it is the one that corresponds to the case of a very widely broadened ionic transition in a crystal.

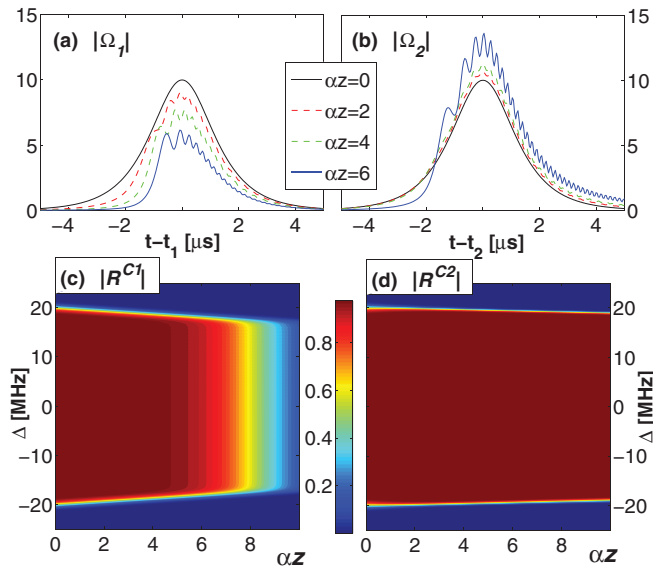


FIG. 4. (Color online) The behavior of two successive frequency-chirped sech control pulses as they propagate in the storage medium with $g(\Delta) = g_0$. Pulse parameters: $\tau = 1 \mu\text{s}$, $\Omega_0 = 10 \text{ MHz}$, and $\mu = -20$. (a),(b) $|\Omega_1(t)|$ and $|\Omega_2(t)|$ (both in MHz) at normalized propagation distances of $\alpha_d z = 0, 2, 4, 6$. (c),(d) contour plots of $|\mathcal{R}^{C1}|$ and $|\mathcal{R}^{C2}|$ vs Δ and $\alpha_d z$.

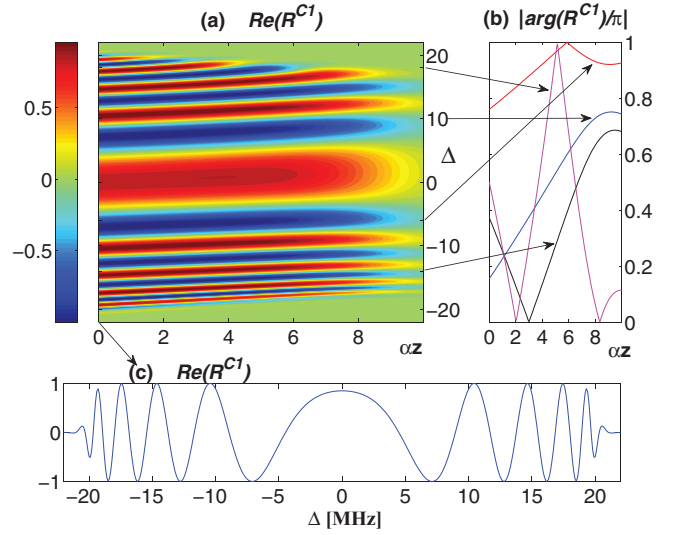


FIG. 5. (Color online) The behavior of \mathcal{R}^{C1} for the first control pulse. (a) Contour plot of $\text{Re}(\mathcal{R}^{C1})$ as a function of Δ (MHz) and $\alpha_d z$. (b) Line plots of $|\arg(\mathcal{R}^{C1})/\pi|$ vs $\alpha_d z$ for $\Delta = -14, -6, 10$, and 18 , indicated by arrows. (c) Line plot of $\text{Re}(\mathcal{R}^{C1})$ vs Δ at $\alpha_d z = 0$. (Pulse parameters are the same as for Fig. 4.)

Figures 4(a) and 4(b) depict how a pair of successive chirped control pulses are deformed during propagation when $g(\Delta) = g_0$. The time plots of the pulse amplitudes show clearly that the first pulse is considerably attenuated, while the second one is amplified. At the same time both pulse amplitudes are modulated in time. Figures 4(c) and 4(d) depict $|\mathcal{R}^{C1}|$ and $|\mathcal{R}^{C2}|$ as functions of Δ and $\alpha_d z$. They show that at $z = 0$ both pulses create AP over roughly the $\Delta \in \{-20 \text{ MHz}, 20 \text{ MHz}\}$ frequency interval, but the range where AP works for the first pulse narrows continuously, and at about $\alpha_d z = 4.5$ it starts deteriorating over the entire frequency range. The second pulse on the other hand maintains AP until the calculated distance of $\alpha_d z = 10$ with only the frequency interval narrowing very slightly. Figure 5 illustrates the rephasing power of the first control pulse, or rather the lack of it. The contour plot of $\text{Re}(\mathcal{R}^{C1})$ [Fig. 5(a)] shows that the phase associated with the transformation of the atomic coherences is not uniform across the ensemble, not even in the domain where the pulse creates AP. It changes with Δ at any given optical depth $\alpha_d z$ and also for any Δ as a function of the optical depth $\alpha_d z$. Line plots of $|\arg(\mathcal{R}^{C1})/\pi|$ for several values of Δ in Fig. 5(b) and of $\text{Re}(\mathcal{R}^{C1})$ at $\alpha_d z = 0$ in Fig. 5(c) demonstrate this even more clearly.

What we have seen so far is just what we anticipated. The surprising result is shown in Fig. 6 where the behavior of $\mathcal{R}^{C1}[\mathcal{R}^{C2}]^*$ has been plotted, the quantity associated with coherence rephasing by a pair of two successive control pulses. Its magnitude, shown in Fig. 6(a), gives the probability that an atom of the ensemble at z and with frequency offset Δ undergoes AP twice as a result of the interaction. This value is close to 1 in an extended region of Δ and $\alpha_d z$ —a region essentially identical to the one in which the first control pulse is able to create AP [see Fig. 5(c)]. Remarkably, the complex phase $\arg(\mathcal{R}^{C1}[\mathcal{R}^{C2}]^*)$ shown in Fig. 6(b) is also essentially constant in this region. The line where $|\mathcal{R}^{C1}[\mathcal{R}^{C2}]^*| = 0.98$

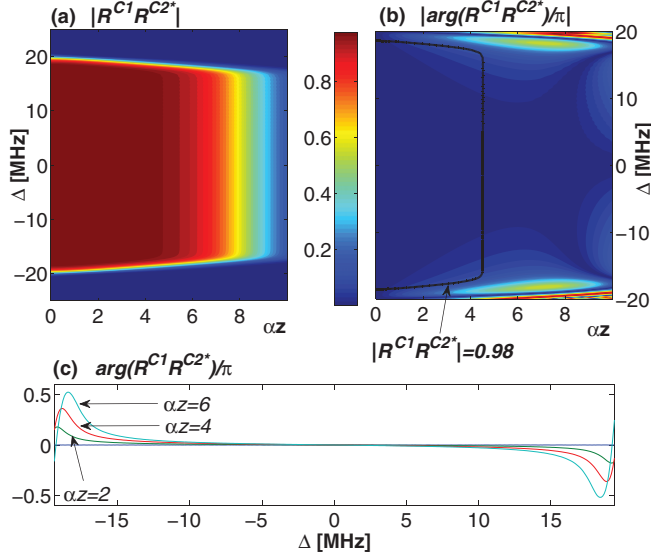


FIG. 6. (Color online) The behavior of $\mathcal{R}^{C1}[\mathcal{R}^{C2}]^*$ for a pair of successive chirped control pulses. (a) Contour plot of $|\mathcal{R}^{C1}[\mathcal{R}^{C2}]^*|$ as a function of Δ and $\alpha_d z$. (b) Contour plot of $|\arg(\mathcal{R}^{C1}[\mathcal{R}^{C2}]^*)/\pi|$ —the heavy black line corresponds to $|\mathcal{R}^{C1}[\mathcal{R}^{C2}]^*| = 0.98$. (c) Line plots of $\arg(\mathcal{R}^{C1}[\mathcal{R}^{C2}]^*)/\pi$ vs Δ at optical depths of $\alpha_d z = 0, 2, 4$, and 6 . (Pulse parameters are the same as for Fig. 4.)

has been drawn over the contour plot for guidance. This means that despite the considerable and unequal distortion the two control pulses suffer during propagation, the pair of chirped pulses can rephase a sizable domain of the atomic ensemble in terms of both optical depth and frequency interval. With these parameters the boundaries are roughly at $\Delta \in \{-15 \text{ MHz}, 15 \text{ MHz}\}$ and $\alpha_d z = 4.5$, but this can be extended easily by increasing the pulse amplitude or the chirp slightly. For example, the same pulses with $\Omega_0 = 12 \text{ MHz}$ instead of $\Omega_0 = 10 \text{ MHz}$ can rephase the coherences to about $\alpha_d z = 8.7$.

For a comparison, we also calculated the rephasing abilities of a pair of consecutive π pulses in an identical way. Naturally, a pulse of much shorter duration and hence much

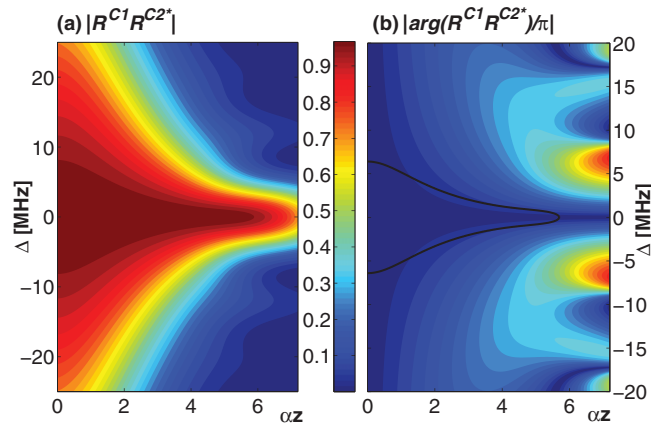


FIG. 7. (Color online) The behavior of $\mathcal{R}^{C1}[\mathcal{R}^{C2}]^*$ for a pair of successive π pulses. (a) Contour plot of $|\mathcal{R}^{C1}[\mathcal{R}^{C2}]^*|$ as a function of Δ and $\alpha_d z$. (b) Contour plot of $|\arg(\mathcal{R}^{C1}[\mathcal{R}^{C2}]^*)/\pi|$ —the heavy black line corresponds to $|\mathcal{R}^{C1}[\mathcal{R}^{C2}]^*| = 0.98$. Pulse parameters: $\tau = 0.01 \mu\text{s}$, $\Omega_0 = 100 \text{ MHz}$, $\mu = 0$.

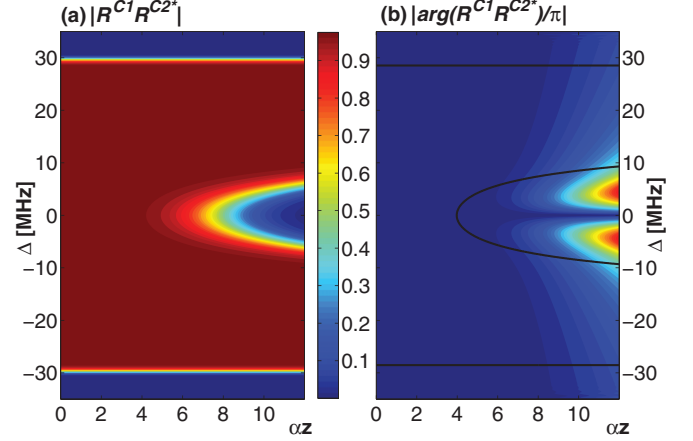


FIG. 8. (Color online) The behavior of $\mathcal{R}^{C1}[\mathcal{R}^{C2}]^*$ for a pair of successive frequency-chirped pulses propagating through a medium with a Gaussian inhomogeneous line shape function with $\sigma_\Delta = 6.2666$. (a) Contour plot of $|\mathcal{R}^{C1}[\mathcal{R}^{C2}]^*|$ as a function of Δ and $\alpha_d z$. (b) Contour plot of $|\arg(\mathcal{R}^{C1}[\mathcal{R}^{C2}]^*)/\pi|$ —the heavy black line corresponds to $|\mathcal{R}^{C1}[\mathcal{R}^{C2}]^*| = 0.98$. Pulse parameters: $\tau = 1 \mu\text{s}$, $\Omega_0 = 12 \text{ MHz}$, $\mu = -30$.

greater peak intensity is needed to rephase a comparable region of the ensemble. Figure 7 shows the contour plots of the magnitude and phase of $\mathcal{R}^{C1}[\mathcal{R}^{C2}]^*$. It is clear that with the chosen parameters ($\tau = 0.01 \mu\text{s}$, $\Omega_0 = 100 \text{ MHz}$, $\mu = 0$) the performance of the π -pulse pair is inferior to that of the chirped-pulse pair. The frequency interval where $|\mathcal{R}^{C1}[\mathcal{R}^{C2}]^*| \approx 1$ is much narrower even at $z = 0$ and narrows rapidly. While the pulse energies are the same with these parameters, the peak intensity of the π pulses is 100 times greater.

One advantage of π pulses is of course that the interaction time is much shorter, and the control works faster. However, because of the long “tail” that the π pulses develop during propagation [5] this advantage is far smaller than the actual difference between the time constants. (For the present case the initial π pulses of $\tau = 0.01 \mu\text{s}$ widen to several times $0.1 \mu\text{s}$ by about $\alpha_d z = 5$ which means that an initial advantage of two orders of magnitude is essentially reduced to one order of magnitude.)

Finally, Fig. 8 depicts $\mathcal{R}^{C1}[\mathcal{R}^{C2}]^*$ for a pair of chirped control pulses that propagate through a medium with a relatively narrow inhomogeneous broadening. $g(\Delta)$ is now a Gaussian with a width of $\sigma_\Delta = 6.2666$, while the chirp range of the pulses is from -30 MHz to 30 MHz , so the control pulses are able to invert the whole atomic ensemble. Figure 8(a) shows that now the ability of the pulse pair to create AP twice is lost only around the central frequencies where the medium is optically the densest. Figure 8(b) shows that, again, $\arg(\mathcal{R}^{C1}[\mathcal{R}^{C2}]^*)$ is almost constant in the region where AP works (the black line again marking the boundary of $|\mathcal{R}^{C1}[\mathcal{R}^{C2}]^*| = 0.98$; a deviation from the constant phase can be observed for $\alpha_d z > 7$).

IV. PHOTON ECHOES

To verify that frequency-chirped control pulses are suitable for applications in photon-echo memories, we used

Eqs. (1)–(3) to calculate the echoes of a set of weak signal pulses and compare them with the original signal. Gaussians of the form $E_s(t) \sim \exp(-t^2/2\tau^2)$ were used with $\tau = 1 \mu\text{s}$, and a variable frequency ω_s , detuned slightly from ω_0 (to which the central frequency of the control pulses was tuned). We performed a parameter scan with respect to ω_s and the optical length of the storage medium $\alpha_d L$ for both variants of the memory protocol described in Sec. II B. We used a classical signal, but assumed that it is so weak that it does not in any way influence the propagation of the strong control pulses. Thus after having calculated the coherences imprinted in the ensemble by the signal, we used the time-evolution operators computed in Sec. III (without a signal) to calculate the atomic states at $t_3 - T$. We then solved Eqs. (1)–(3) again numerically for the time interval $[t_3 - T, t_3 + T]$ to obtain the echo.

The efficiency of the memory protocol with chirped pulses was then characterized by calculating the ratio of echo energy to signal energy:

$$\eta = \frac{\int |E_e(t)|^2 dt}{\int |E_s(t)|^2 dt}, \quad (8)$$

which, in the weak-signal limit corresponds to the overall probability that an incident photon is absorbed by the medium and later reemitted as a signal echo. Another figure of merit calculated was a classical fidelity

$$\xi = \max_{t_{\text{delay}}} \left| \frac{\int E_e(t - t_{\text{delay}}) E_s^*(t) dt}{\sqrt{\int |E_s(t)|^2 dt \int |E_e(t)|^2 dt}} \right| \quad (9)$$

which characterizes the similarity of the signal and echo fields, neglecting an arbitrary difference in phase and reduction in amplitude.

Our calculation of the echo field includes all of the atomic ensemble, those atoms that undergo AP twice during the interaction with the control pulses, and also those that do not. Atoms that are too far either in optical depth $\alpha_d z$ or in frequency offset Δ to be rephased may still contribute during echo emission, possibly to distort the signal. However, the calculation is entirely classical, so it does not account for quantum noise, such as spontaneously emitted photons from atoms that, due to imperfect AP, are left in the excited state after the second control pulse. The classical fidelity presented here cannot be identified with the true fidelity of a one- (few-) photon signal pulse.

Figures 9–12 depict our results. In each figure, (a) shows a contour plot of the efficiency η as a function of signal detuning $\omega_s - \omega_0$ and optical length $\alpha_d L$. The results are symmetric with respect to $\omega_s - \omega_0$, so only negative values have been plotted for a better visibility. (b) in each figure shows η for two specific values of $\omega_s - \omega_0$ along with the curves of the best theoretical efficiency calculated for CRIB [13]: $\eta' = (1 - e^{-\alpha_d L})^2$ for backward echo emission and $\eta' = (\alpha_d L)^2 e^{-\alpha_d L}$ for forward echo emission. In each figure, (c) is a plot of η and the fidelity ξ as functions of $\omega_s - \omega_0$ for a given optical length. Figures 9 and 10 show that when we have $g(\Delta) = g_0$, η is practically constant at any $\alpha_d L$ for a wide range of signal detunings. The efficiencies for $\omega_s = \omega_0$ lie precisely on the curves for η' , and even $\omega_s - \omega_0 = -16$ MHz yields efficiencies just very slightly below them. The fidelity

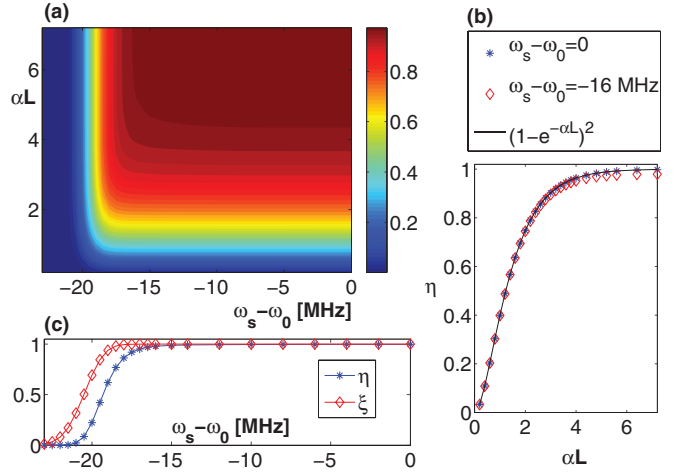


FIG. 9. (Color online) Memory efficiency and fidelity for backward echo emission and $g(\Delta) = g_0$. (a) η vs optical length $\alpha_d L$ and signal detuning $\omega_s - \omega_0$. (b) η vs $\alpha_d L$ for $\omega_s - \omega_0 = 0$ (blue *), $\omega_s - \omega_0 = -16$ MHz (red \diamond), and $\eta' = (1 - e^{-\alpha_d L})^2$ (solid line). (c) η and ξ vs $\omega_s - \omega_0$ at $\alpha_d L = 7.2$. Control-pulse parameters are identical to those in Figs. 4–6.

ξ is also extremely close to unity in this region. Both η and ξ start to decrease only when the boundary of the control pulse frequency range (between -20 MHz and 20 MHz) is approached. For backward echos, $\eta_{\text{max}} = 1$ with $\eta = 0.9985$ being reached by $\alpha_d L = 7.2$ depicted in Figs. 9(b) and 9(c), while for forward echos $\eta_{\text{max}} = 0.54$ at $\alpha_d L = 2$ [Figs. 10(b) and 10(c)]. The reason for the reduction of η_{max} for forward echos is the same as in the case of CRIB—the echo is reabsorbed again by the storage medium if it is too thick.

Figures 11 and 12 show the case when we have a Gaussian $g(\Delta)$. Backward echo efficiency now approaches $\eta_{\text{max}} = 1$ only for $\omega_s = \omega_0$ and is considerably less for a signal detuning of $\omega_s - \omega_0 = -5$ MHz already [Figs. 11(a)

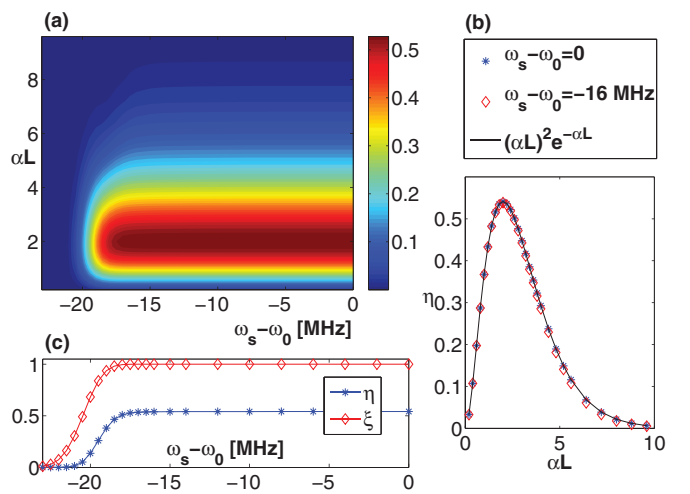


FIG. 10. (Color online) Memory efficiency and fidelity for forward echo emission and $g(\Delta) = g_0$. (a) η vs optical length $\alpha_d L$ and signal detuning $\omega_s - \omega_0$. (b) η vs $\alpha_d L$ for $\omega_s - \omega_0 = 0$ (blue *), $\omega_s - \omega_0 = -16$ MHz (red \diamond), and $\eta' = (\alpha_d L)^2 e^{-\alpha_d L}$ (solid line). (c) η and ξ vs $\omega_s - \omega_0$ at $\alpha_d L = 2$. Control-pulse parameters are identical to those in Figs. 4–6.

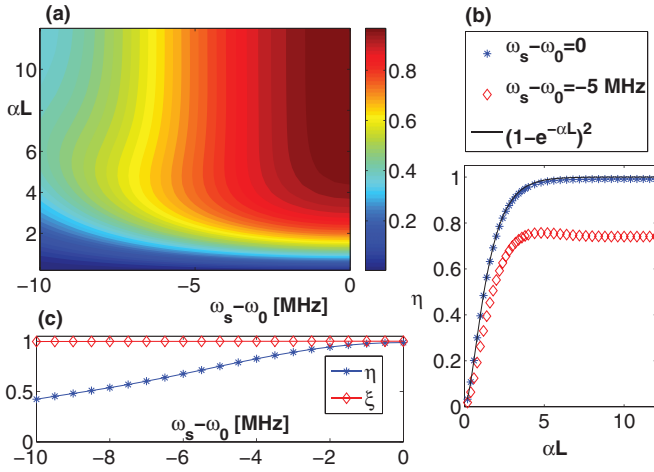


FIG. 11. (Color online) Memory efficiency and fidelity for backward echo emission and $g(\Delta)$ a Gaussian. (a) η vs optical length $\alpha_d L$ and signal detuning $\omega_s - \omega_0$. (b) η vs $\alpha_d L$ for $\omega_s - \omega_0 = 0$ (blue *), $\omega_s - \omega_0 = -5$ MHz (red \diamond), and $\eta' = (1 - e^{-\alpha_d L})^2$ (solid line). (c) η and ξ vs $\omega_s - \omega_0$ at $\alpha_d L = 6$. Control-pulse parameters are identical to those in Fig. 8.

and 11(b)]. Forward echo efficiency does approach $\eta_{\max} = 0.54$ for a wider range of detunings, but the storage medium length which is required is greater for a signal detuned from ω_0 [Figs. 12(a) and 12(b)]. This is because with a relatively narrow broadening ($\sigma_\Delta = 6.2666$) a signal detuned from the atomic line center experiences a reduced optical length. For the same reason, at a given medium length, the efficiency η decreases with $|\omega_s - \omega_0|$. At the same time Figs. 11(c) and 12(c) show that the echo signal is only reduced but not distorted; ξ remains close to 1.

Some comments on possible control-pulse parameters are in order. First of all, decoherence effects other than dephasing due to inhomogeneous broadening have been neglected in

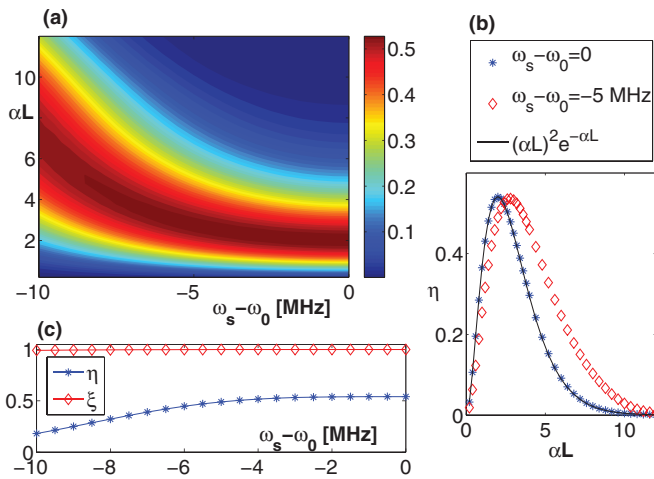


FIG. 12. (Color online) Memory efficiency and fidelity for forward echo emission and $g(\Delta)$ a Gaussian. (a) η vs optical length $\alpha_d L$ and signal detuning $\omega_s - \omega_0$. (b) η vs $\alpha_d L$ for $\omega_s - \omega_0 = 0$ (blue *), $\omega_s - \omega_0 = -5$ MHz (red \diamond), and $\eta' = (\alpha_d L)^2 e^{-\alpha_d L}$ (solid line). (c) η and ξ vs $\omega_s - \omega_0$ at $\alpha_d L = 2$. Control-pulse parameters are identical to those in Fig. 8.

our description. Because there are no other “inherent” time scales, the results presented apply equally well to any other parameter set which is scaled consistently (pulse lengths, Rabi frequencies, chirp parameters, and atomic frequency offsets must be scaled together). Naturally, the time delay between the control pulses (which is half the memory storage time without the auxiliary shelving state $|s\rangle$) cannot be more than a few percent of the excited-state lifetime Γ^{-1} for our results to remain valid. While control pulses of arbitrary τ can satisfy the requirements of AP, the upper bound will be set by $\tau^{\max} \sim 10^{-3} \Gamma^{-1}$. AP requires that the pulse area of the real envelope function be $\mathcal{A} = \int |\Omega(t)| dt \gtrsim 10\pi$. (The precise value of course depends slightly on the pulse shape and the chirp function; in our case $\mathcal{A} = 10\pi$ proved entirely sufficient.) Together with the constraint on τ^{\max} , this sets the lower bound of the peak Rabi frequency to be $\Omega_0^{\min} \gtrsim 10^4 \Gamma$.

The ideal choice for the chirp parameter is such that the full bandwidth of the pulse is at least a few times Ω_0 . Much lower values are impractical, because then the extension of the transition region in Δ where the control pulses perturb the atoms but AP fails is comparable to the region where AP works correctly. (The significance of this will be clarified shortly.) τ^{\min} and μ^{\max} will be set by the requirement that the full control-pulse bandwidth cannot exceed the distance to the nearest unused electronic level. This then constrains Ω_0^{\max} as well. It may well happen, however, that this Ω_0^{\max} already corresponds to a peak intensity that is either too high to generate or for the medium (host crystal) to endure. In this case the latter constraint on Ω_0^{\max} obtains precedence and sets τ^{\min} via the requirement on \mathcal{A} .

Regarding the possible range of optical depths one may consider, we note that due to the exponential decay of the signal during absorption, a medium with $\alpha_d L = 5-10$ is perfectly sufficient to absorb the signal. Thus we need not consider optical depths of $\alpha_d L > 10$ and, indeed, the ideal choice for forward echo emission is $\alpha_d L = 2$. In our simulations $\Omega_0 = 10$ MHz rephases atoms of the ensemble almost perfectly until about $\alpha_d z = 4.5$, which is already sufficient for an excellent memory efficiency. However, this limit can easily be extended if necessary— $\Omega_0 = 12$ MHz rephases the ensemble to $\alpha_d z = 8.7$, $\Omega_0 = 14$ MHz to well above $\alpha_d z = 10$.

A. Further implications for photon-echo memories

In light of these results, it is clear that a pair of chirped control pulses that drive AP are better for building quantum memories than a pair of π pulses for several reasons. The first one mentioned already in the Introduction is of course that pulses with much smaller peak intensity can be used. [In Sec. III the particular example showed that chirped pulses with two orders of magnitude smaller peak intensity deliver far better rephasing ability for the case of constant $g(\Delta)$.]

The second advantage is the small width of the transition region in frequency where atoms are not perfectly rephased, but nevertheless considerably perturbed by the control pulses. When we have a widely broadened inhomogeneous line and can hope to rephase only a relatively narrow frequency region (which is in fact the generic case in rare-earth-doped crystals), this is very important because atoms that are not inverted twice perfectly may remain excited after the second control

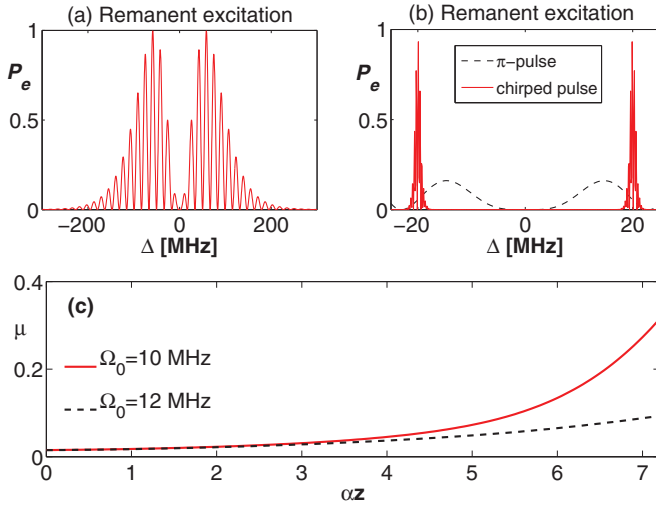


FIG. 13. (Color online) Remanent excitation in the medium after the two control pulses at $\alpha_d z = 0$ for π pulses [(a) and dashed line in (b)] and chirped pulses [solid line in (b)] as functions of Δ . Pulse parameters are the same as for Figs. 4 and 7. (c) The ratio μ of the overall excitation left in the medium by the chirped control pulses and the π control pulses as a function of optical depth for two different chirped-pulse amplitudes.

pulse. They will then be a source of noise due to spontaneous emission at the time of signal retrieval. (It is important to note that even though the duration T_{mem} of the whole sequence may be $T_{\text{mem}} \ll \Gamma^{-1}$, the question of spontaneous emission during echo emission must still be considered, at least qualitatively. Because the ultimate goal is to retrieve a single photon pulse, if there are a large number of excited atoms in the ensemble at retrieval time, spontaneous emission may be detrimental, however short the signal pulse is [5].)

To assess the reduction in spontaneous noise more quantitatively, we compute the probabilities that atoms remain in the excited state after the second— π or chirped—control pulse, the “remanent excitation” due to the control pulses $P_e^\pi(\Delta, z)$ and $P_e^C(\Delta, z)$. This quantity can be extracted from the time-evolution operator used earlier:

$$P_e(\Delta, z) = |[\hat{U}(\Delta, z)]_{2,1}|^2.$$

The plot of $P_e^\pi(\Delta)$ at $\alpha_d z = 0$ for a pair of π pulses can be seen in Fig. 13(a), which shows two wide regions of remanent excitation one on each side of the narrow central hole. This latter is the region where atoms are correctly rephased, while the fast oscillations on both sides trace out a slow envelope of two wide maxima. The precise frequency and phase of the rapid oscillations depend on the time between the two control pulses; the width of the slow envelope however depends only on their bandwidth. In this case, $\tau = 0.01 \mu\text{s}$ has been used (as for Fig. 7), so the width of the high- P_e^π region is about 100 MHz. $P_e^C(\Delta)$ is shown by the solid line in Fig. 13(b), which again shows a rapidly oscillating curve that traces out two relatively narrow maxima at $\Delta = \pm 20$ MHz. (The pulse parameters used were the same as for Figs. 4–6: $\tau = 1 \mu\text{s}$, $\Omega_0 = 10$ MHz, and $\mu = -20$.) The width of the maxima is approximately 1 MHz, the bandwidth of the pulse due solely to its duration, while their positions are at the two limits of the

full frequency range of the chirped pulse. The dashed curve between the two sharp maxima is the plot of the very central part of $P_e^\pi(\Delta)$ from Fig. 13(a), plotted to show that with these parameters, the π -pulse pair rephases atoms only in a much smaller frequency range.

To characterize the reduction in spontaneous noise due to atoms in the transition region, we calculate $\mu = \int P_e^C(\Delta) d\Delta / \int P_e^\pi(\Delta) d\Delta$, the ratio of the overall excitation remaining in the two cases. This quantity is shown with a solid line in Fig. 13(c); its initial value at $\alpha_d z = 0$ is $\mu = 0.015$. It increases very slightly at first with the optical depth, because as the π pulse loses energy its bandwidth decreases and thus the width of the transition region narrows somewhat. At around the point where AP for the first chirped control pulse starts failing ($\alpha_d z = 4.5$ in this case) μ starts increasing much faster because the second chirped pulse then starts leaving more and more atoms in the excited state for every Δ within its bandwidth. At $\alpha_d z = 4.5$ we have $\mu = 0.056$, so spontaneous noise due to remanent excitation at this point is still about 18 times less for the chirped pulses. The optical depth to which AP works can also be extended easily with slightly larger pulse amplitudes— μ calculated with a chirped-pulse amplitude of $\Omega_0 = 12$ MHz is shown with a broken line in Fig. 13(c). We also note that for the comparison we used π pulses which are capable of rephasing a far smaller frequency domain within the ensemble to start with. [The width of the central region where atoms are rephased is only about 12 MHz, while it is close to 34 MHz for the chirped pulses; see Fig. 13(b). Also compare Figs. 6 and 7.] Altogether it is safe to say that spontaneous-emission-induced noise can be reduced by a factor of 10^{-2} if we use chirped control pulses instead of π pulses with comparable rephasing ability.

For a relatively narrow $g(\Delta)$ it is of course possible to choose control pulses where the whole atomic ensemble is inverted, i.e., the transition region lies in a spectral domain void of absorbers. Then its width is not important. However, unmanipulated ionic transition lines in solids are usually broad. A narrow absorption feature (of a few megahertz in width as used in Sec. III) would have to be prepared using techniques identical to those used for CRIB.

One may also envision devices where the same storage medium is used for several distinct “memory channels” of different frequencies, manipulated separately by control pulses. In this case, one clearly has to maintain a spectral distance between the channels such that they do not interfere with each other—“cross-talk” between the channels must be kept low. This means that the interchannel spectral distance is constrained by the width of the transition region. Chirped pulses clearly have a much greater potential in this field.

V. SUMMARY AND CONCLUSION

In this paper, we have investigated the ability of a pair of chirped control pulses to rephase the coherences in an inhomogeneously broadened, optically thick ensemble of two-level atoms. By solving the Maxwell-Bloch equations numerically, we have shown that as long as both pulses drive AP between the atomic states, they can collectively rephase the atomic coherences. This result is somewhat counterintuitive, because the time integral of the adiabatic eigenvalues plays

an important role in rephasing and the two successive pulses evolve differently as they propagate through the medium. The first pulse is attenuated because of absorption, while the second one, propagating in the gain medium prepared by the first one, is amplified. Nevertheless, there is a well-defined region in the ensemble in terms of atomic frequency and optical depth, where rephasing works well. The extent of this region is considerably greater than that rephased by a pair of consecutive π pulses with the same energy, but two orders of magnitude higher peak intensity, which is an important property when rare-earth-ion impurities embedded in a crystal are used as a storage medium. The price to pay is a somewhat longer control-pulse time, which, however, is only about one order of magnitude greater after pulse propagation effects are taken into account.

We have shown that it is possible to use chirped control pulses in photon-echo memory schemes, where the primary echo after the first control pulse is silenced by spatial phase mismatching. The atomic coherences rephase again after the second control pulse, this time without the storage medium being inverted. Using chirped control pulses, the same maximum echo efficiencies are theoretically attainable in an unmanipulated, naturally inhomogeneously broadened ensemble, as in schemes such as CRIB or AFC. For these latter schemes numerous preparatory steps are required to obtain the absorption feature required by the protocol. For chirped control pulses, the frequency width of the transition region where the control pulses excite the atoms considerably, but fail to rephase them properly, can be relatively small. This means that quantum noise emanating from it (atoms left in their excited states by the control pulses emitting photons spontaneously during echo emission) could be small enough for the retrieval of quantum information.

It is also possible to use an ensemble with great inhomogeneous width for the storage of several memory channels with different frequencies simultaneously. Because of the narrow transition region, using chirped pulses means that a much smaller frequency distance between the distinct channels is needed to suppress cross-talk between them. This allows multimode information storage with the separate, on-demand, recall of the information stored in different channels. The same with a pair of π pulses would not be possible, for the width of the disturbing transition region is orders of magnitude greater.

APPENDIX: CONSTRUCTION OF THE TIME-EVOLUTION OPERATOR

Let us regard an atom at z and with frequency offset Δ , such that it is well within the frequency range spanned by the spectrum of the control pulse. $\hat{U}(\Delta, z)$ propagates the probability amplitudes from $t_0 + T$ to $t_3 - T$ as

$$\begin{pmatrix} \alpha'_n \\ \beta'_{n\pm 1} \end{pmatrix} = \hat{U}(\Delta, z)(\alpha_n \beta_{n\pm 1}),$$

where T is a time of about the same order of magnitude as the signal length, sufficiently long that the signal field has effectively decayed to zero everywhere in the medium. $\hat{U}(\Delta, z)$ can be constructed from the operators for free evolution between the pulses \hat{U}^{F1} , \hat{U}^{F2} , and \hat{U}^{F3} and those for the

control pulses $\hat{U}^{C1}(\Delta, z)$ and $\hat{U}^{C2}(\Delta, z)$ as

$$\hat{U}(\Delta, z) = \hat{U}^{F3} \hat{U}^{C2}(\Delta, z) \hat{U}^{F2} \hat{U}^{C1}(\Delta, z) \hat{U}^{F1}. \quad (\text{A1})$$

Here \hat{U}^{F1} , \hat{U}^{F2} , and \hat{U}^{F3} correspond to free evolution during the time intervals $[t_0 + T, t_1 - T']$, $[t_1 + T', t_2 - T']$, and $[t_2 + T', t_3 - T]$, respectively, and $\hat{U}^{C1}(\Delta, z)$ and $\hat{U}^{C2}(\Delta, z)$ to evolution during the intervals $[t_1 - T', t_1 + T']$ and $[t_2 - T', t_2 + T']$. The time parameter T' plays the same role as T does for the signal pulse—it is chosen such that the control fields are effectively zero outside the intervals $[t_j - T', t_j + T']$. For any $[t, t']$, \hat{U}^F is given by

$$\hat{U}^F = \begin{pmatrix} 1 & 0 \\ 0 & e^{-i\Delta(t'-t)} \end{pmatrix}. \quad (\text{A2})$$

To construct $\hat{U}^{C1}(\Delta, z)$ it is convenient to introduce the real envelope and phase functions as $\Omega_1(t) = A_1(t)e^{-i\Phi_1(t)}$ and transform to a reference frame that rotates with the instantaneous frequency of the pulse, using

$$\hat{R}_1^\dagger(t) = \begin{pmatrix} 1 & 0 \\ 0 & e^{i\Phi_1(t)} \end{pmatrix}.$$

Then the equations for $\alpha_r(t) = \alpha(t)$ and $\beta_r(t) = \beta(t)e^{i\Phi_1(t)}$ become

$$\partial_t \begin{pmatrix} \alpha_r \\ \beta_r \end{pmatrix} = i \begin{pmatrix} 0 & A_1(t)/2 \\ A_1(t)/2 & \delta(t) \end{pmatrix} \begin{pmatrix} \alpha_r \\ \beta_r \end{pmatrix}, \quad (\text{A3})$$

where we have introduced the instantaneous detuning perceived by the atom, $\delta(t) = \partial_t \Phi_1(t) - \Delta$. The Hamiltonian matrix in Eq. (A3) can be diagonalized by transforming to the reference frame of the instantaneous eigenvectors in the standard way [29]:

$$\begin{pmatrix} q^+(t) \\ q^-(t) \end{pmatrix} = \hat{V}^\dagger \begin{pmatrix} \alpha_r(t) \\ \beta_r(t) \end{pmatrix},$$

where \hat{V} is given by

$$\hat{V} = \begin{pmatrix} \cos \theta & -\sin \theta \\ \sin \theta & \cos \theta \end{pmatrix}$$

$$\text{with } \sin \theta = \frac{A_1}{\sqrt{(\mathcal{R} - \delta)^2 + A_1^2}}, \quad \cos \theta = \frac{\mathcal{R} - \delta}{\sqrt{(\mathcal{R} - \delta)^2 + A_1^2}},$$

$$\text{and } \mathcal{R} = \sqrt{A_1^2 + \delta^2}.$$

Then (A3) becomes

$$\partial_t \begin{pmatrix} q^+ \\ q^- \end{pmatrix} = i \begin{pmatrix} \lambda^+ & 0 \\ 0 & \lambda^- \end{pmatrix} \begin{pmatrix} q^+ \\ q^- \end{pmatrix} + (\partial_t \hat{V}^\dagger \hat{V}) \begin{pmatrix} q^+ \\ q^- \end{pmatrix}, \quad (\text{A4})$$

where the first term on the right-hand side contains the adiabatic eigenvalues $\lambda^\pm = \frac{1}{2}(\delta \pm \mathcal{R})$ and the second term describes nonadiabatic transitions due to the finite rotation

speed of the basis:

$$\partial_t \hat{V}^\dagger \hat{V} = \begin{pmatrix} 0 & \partial_t \theta \\ -\partial_t \theta & 0 \end{pmatrix}.$$

If we neglect nonadiabatic transitions, we can solve (A4) to obtain the time-evolution operator in this frame as

$$\hat{U}_{AP}^{C1} = \begin{pmatrix} e^{i\Lambda_1^+} & 0 \\ 0 & e^{i\Lambda_1^-} \end{pmatrix} \quad \text{where} \quad \Lambda_1^\pm = \int_{t_1-T'}^{t_1+T'} \lambda^\pm(t') dt'. \quad (\text{A5})$$

The Λ_1^\pm depend on Δ through λ^\pm , as well as the precise time evolution of $A_1(t)$ and $\partial_t \Phi_1$.

We now assume that the frequency modulation is positive, so $\delta(t_1 - T') < 0$ and $\delta(t_1 + T') > 0$. Then $\sin \theta|_{t_1-T'} = 0$, $\cos \theta|_{t_1-T'} = 1$ and $\sin \theta|_{t_1+T'} = 1$, $\cos \theta|_{t_1+T'} = 0$, so in the

original reference frame we obtain

$$\begin{aligned} \hat{U}_{(\Delta,z)}^{C1} &= \hat{R}_1(t_1 + T') \hat{V}(t_1 + T') \hat{U}_{AP}^{C1} \hat{V}^\dagger(t_1 - T') \hat{R}_1^\dagger(t_1 - T') \\ &= \begin{pmatrix} 0 & e^{i\Lambda_1^-} e^{i\Phi_1(t_1-T')} \\ -e^{i\Lambda_1^+} e^{-i\Phi_1(t_1+T')} & 0 \end{pmatrix}. \end{aligned} \quad (\text{A6})$$

An identical construction for the second control pulse $\hat{U}_{(\Delta,z)}^{C2}$ and a substitution of (A2) and (A6) into (A1) yields

$$\begin{aligned} [\hat{U}_{(\Delta,z)}]_{11} &= -e^{i[\Lambda_1^+ + \Lambda_2^- + \Phi_2(t_2-T') - \Phi_1(t_1+T') - i\Delta(t_2-t_1-2T')]} \\ [\hat{U}_{(\Delta,z)}]_{22} &= -e^{i[\Lambda_2^+ + \Lambda_1^- + \Phi_1(t_1-T') - \Phi_2(t_2+T') - i\Delta(t_1-t_0+t_3-t_2-2T-2T')]} \\ [\hat{U}_{(\Delta,z)}]_{12} &= [\hat{U}_{(\Delta,z)}]_{21} = 0 \end{aligned} \quad (\text{A7})$$

for the matrix elements of $\hat{U}(\Delta, z)$ when the conditions for adiabatic passage are fulfilled.

-
- [1] A. I. Lvovsky, B. C. Sanders, and W. Tittel, *Nat. Photon.* **3**, 706 (2009).
- [2] C. Simon, M. Afzelius, J. Appel, A. B. de La Giroday, S. Dewhurst, N. Gisin, C. Hu, F. Jelezko, S. Kröll, J. Müller *et al.*, *Eur. Phys. J. D* **58**, 1 (2010).
- [3] W. Tittel, M. Afzelius, T. Chanelière, R. Cone, S. Kröll, S. Moiseev, and M. Sellars, *Laser Photon. Rev.* **4**, 244 (2010).
- [4] L. Allen and J. H. Eberly, *Optical Resonance and Two-Level Atoms* (Dover Publications, New York, 1987).
- [5] J. Ruggiero, J.-L. Le Gouët, C. Simon, and T. Chanelière, *Phys. Rev. A* **79**, 053851 (2009).
- [6] J. Ruggiero, T. Chanelière, and J. Le Gouët, *J. Opt. Soc. Am. B* **27**, 32 (2010).
- [7] N. Sangouard, C. Simon, J. Minář, M. Afzelius, T. Chanelière, N. Gisin, J.-L. Le Gouët, H. de Riedmatten, and W. Tittel, *Phys. Rev. A* **81**, 062333 (2010).
- [8] V. Damon, M. Bonarota, A. Louchet-Chauvet, T. Chanelière, and J. Le Gouët, *New J. Phys.* **13**, 093031 (2011).
- [9] B. S. Ham, *Phys. Rev. A* **85**, 031402 (2012).
- [10] S. A. Moiseev, *Phys. Rev. A* **83**, 012307 (2011).
- [11] D. L. McAuslan, P. M. Ledingham, W. R. Naylor, S. E. Beavan, M. P. Hedges, M. J. Sellars, and J. J. Longdell, *Phys. Rev. A* **84**, 022309 (2011).
- [12] B. Kraus, W. Tittel, N. Gisin, M. Nilsson, S. Kröll, and J. I. Cirac, *Phys. Rev. A* **73**, 020302(R) (2006).
- [13] N. Sangouard, C. Simon, M. Afzelius, and N. Gisin, *Phys. Rev. A* **75**, 032327 (2007).
- [14] J. J. Longdell, G. Hétet, P. K. Lam, and M. J. Sellars, *Phys. Rev. A* **78**, 032337 (2008).
- [15] S. A. Moiseev and N. M. Arslanov, *Phys. Rev. A* **78**, 023803 (2008).
- [16] G. Hétet, J. J. Longdell, A. L. Alexander, P. K. Lam, and M. J. Sellars, *Phys. Rev. Lett.* **100**, 023601 (2008).
- [17] A. L. Alexander, J. J. Longdell, M. J. Sellars, and N. B. Manson, *Phys. Rev. Lett.* **96**, 043602 (2006).
- [18] M. U. Staudt, S. R. Hastings-Simon, M. Nilsson, M. Afzelius, V. Scarani, R. Ricken, H. Suche, W. Sohler, W. Tittel, and N. Gisin, *Phys. Rev. Lett.* **98**, 113601 (2007).
- [19] M. P. Hedges, J. J. Longdell, Y. Li, and M. J. Sellars, *Nature (London)* **465**, 1052 (2010).
- [20] F. Carreño and M. Antón, *Opt. Commun.* **284**, 3154 (2011).
- [21] M. Hosseini, B. Sparkes, G. Campbell, P. Lam, and B. Buchler, *J. Phys. B* **45**, 124004 (2012).
- [22] D. Viscor, A. Ferraro, Y. Loiko, J. Mompart, and V. Ahufinger, *Phys. Rev. A* **84**, 042314 (2011).
- [23] D. Viscor, A. Ferraro, Y. Loiko, R. Corbalán, J. Mompart, and V. Ahufinger, *J. Phys. B* **44**, 195504 (2011).
- [24] M. Afzelius, C. Simon, H. de Riedmatten, and N. Gisin, *Phys. Rev. A* **79**, 052329 (2009).
- [25] H. De Riedmatten, M. Afzelius, M. U. Staudt, C. Simon, and N. Gisin, *Nature (London)* **456**, 773 (2008).
- [26] J. Minář, N. Sangouard, M. Afzelius, H. de Riedmatten, and N. Gisin, *Phys. Rev. A* **82**, 042309 (2010).
- [27] M. F. Pascual-Winter, R.-C. Tongning, T. Chanelière, and J. Le Gouët, *New J. Phys.* **15**, 055024 (2013).
- [28] S. Mieth, D. Schraft, T. Halfmann, and L. P. Yatsenko, *Phys. Rev. A* **86**, 063404 (2012).
- [29] P. Meystre and M. Sargent, III, *Elements of Quantum Optics* (Springer-Verlag Berlin, Heidelberg, 2007).